Available online at www.sciencedirect.com
ScienceDirect
Trans. Nonferrous Met. Soc. China 25(2015) 2221−2229
Transactions of Nonferrous Metals Society of China
www.tnmsc.cn

Mechanical properties and microstructural evolution of ultrafine grained zircaloy-4 processed through multiaxial forging at cryogenic temperature

D. FULORIA[1], S. GOEL[1], R. JAYAGANTHAN[1], D. SRIVASTAVA[2], G. K. DEY[2], N. SAIBABA[3]

1. Department of Metallurgical and Materials Engineering, Centre of Nanotechnology IIT Roorkee, Roorkee 247667, India;
2. Materials Science Division, Bhabha Atomic Research Center, Mumbai 40085, India;
3. Nuclear Fuel Complex Limited, Hyderabad 501301, India

Received 7 August 2014; accepted 23 December 2014

Abstract: The mechanical properties and microstructural evolution of zircaloy-4 subjected to cumulative strains of 1.48, 2.96, 4.44 and 5.91 through multiaxial forging (MAF) at cryogenic temperature (77 K) were investigated. The mechanical properties of the MAF treated alloy were measured through universal tensile testing and Vickers hardness testing equipment. The zircaloy-4 deformed up to a cumulative strain of 5.91 showed improvement in both ultimate tensile strength and hardness from 474 MPa to 717 MPa and from HV 190 to HV 238, respectively, as compared with the as-received alloy. However, there was a noticeable decrement in ductility (from 18% to 3.5%) due to the low strain hardening ability of deformed zircaloy-4. The improvement in strength and hardness of the deformed alloy is attributed to the grain size effect and higher dislocation density generated during multiaxial forging. The microstructural evolutions of deformed samples were characterized by optical microscopy and transmission electron microscopy (TEM). The evolved microstructure at a cumulative strain of 5.91 obtained after MAF up to 12 cycles depicted the formation of ultrafine grains with an average size of 150−250 nm.

Key words: zircaloy-4; multiaxial forging; cryogenic temperature; ultrafine-grain; microstructural evolution; mechanical properties

1 Introduction

There is an ever growing demand on the development of ultrafine-grained (UFG) [1] metallic materials for structural applications owing to their improved mechanical and physical properties as compared with their bulk alloys. Severe plastic deformation techniques, such as equal channel angular processing (ECAP) [1−3], high pressure torsion (HPT), cyclic extrusion compression (CEC) [1,2], accumulative roll bonding (ARB) [1,2,4,5] and equal channel angular extrusion (ECAE) [6,7] with the potential for intense straining are employed to obtain UFG (<500 nm), or nanocrystalline (<100 nm) [8] materials. Although these techniques have been extensively used to produce thermally stable ultrafine/nanostructured grain morphology with improved mechanical properties [9], the short-comings are due to the requirement of expensive and complicated die design and low productivity associated with these methods [10].

Multiaxial forging (MAF) is one of the severe plastic deformation techniques applied in the first half of the 1990s with the aim of achieving UFG microstructure in the bulk billets. It is defined as multiple steps of free forging operations by changing the axes of the applied load through 90° [1]. This technique has been successful at room temperature to elevated temperatures for magnesium and its alloys [11,12].

PADAP et al [13] reported improvement in mechanical properties with reduction in grain size from 17 to 0.6 μm in warm MAF of AISI 1016 steel. RAO et al [14] studied multidirectional forging (MDF) of AA6061 alloy at liquid nitrogen temperature and observed the enhancement in mechanical properties due to the formation of ultrafine-grain microstructure with an average grain size of 250 nm. CHERUKURI and SRINIVASAN [15] observed the fine grain structure with similar trends in mechanical properties as obtained by ECAP in MAF AA6061 at room temperature. TANG et al [16] studied MDF of Mg−10Gd−4.8Y−0.6Zr alloy at 773 K. ZHEREBTSOV et al [17] reported UFG

Corresponding author: R. JAYAGANTHAN; Tel: +91-133-2285869; Fax: +91-133-2285243; E-mail: rjayafmt@iitr.ernet.in
DOI: 10.1016/S1003-6326(15)63835-3

evolution with 33% increment in strength in two-phase Ti−6Al−4V alloy. BELYAKOV et al [18] studied strain-induced grain evolution of pure copper by multiple compressions at room temperature.

Deformation at cryogenic temperature (CT) has also been effective in producing UFG structure in various alloys by suppressing dynamic recovery [19], which in turn accumulates the high density defects in the deformed material, leading to an improvement in mechanical properties. Zirconium and its alloys deformed at cryogenic temperature through cryorolling have shown a remarkable improvement in mechanical properties due to grain refinement as per the Hall−Petch relation [20]. GUO et al [21−23] reported improvement in both strength and toughness of Zr processed at different rolling strain rates using cryorolling as compared with bulk Zr. They have also reported substantial improvement in ductility of cryorolled Zr subjected to annealing and attributed it to the formation of multimodal microstructure and increased strain hardening ability in the alloy. SHI et al [24] also reported improvement in both strength and ductility due to the multimodal grain structure in cryorolled pure Zr followed by two-step annealing. KAMALNATH and SARKAR [25] observed optimum strength and ductility between 20%−50% cryorolled zircaloy-2.

Zirconium and its alloys are extensively used in the nuclear industry as in-core structural components of nuclear reactors [26]. In order to ensure the reliability of the components fabricated by Zr alloys under hostile reactor environmental condition, these alloys ought to meet the stringent requirement of excellent physical properties, mechanical properties and close dimensional tolerances [27]. The in-service performance of zircaloy-4 used for cladding the nuclear fuel pellets depends upon the grain size distribution, crystallographic texture, nature and distribution of precipitates and grain morphology [28]. The evolution of these microstructural features is associated with the type and the level of thermomechanical processing of these alloys. Therefore, it is imperative to have an effective processing route that may result in suitable microstructure which enhances the mechanical properties of the alloy. The literature on severe plastic deformation of zirconium and its alloys at cryogenic temperature is scarce and there is no attempt so far on the grain refinement of zircaloy-4 by using MAF at cryogenic temperature. Therefore, the aim of the present work is to achieve the maximum grain refinement in zircaloy-4 via MAF and to study its mechanical behavior through hardness and tensile test. The microstructural evolution of MAF treated zircaloy-4 is characterized by optical microscopy and TEM.

2 Experimental

2.1 Sample preparation

Zircaloy-4 used in the present study was procured from NFC, Hyderabad, India. The alloy was procured as hot-extruded rods with an initial average grain size of 58 μm. The chemical composition of the alloy is listed in Table 1. The samples were machined in prismatic shape of 33 mm × 31 mm × 28 mm from the extruded rods.

Table 1 Chemical composition of zircaloy-4 (mass fraction, %)

Sn	Fe	Cr	Zr
1.5	0.2	0.1	Bal.

2.2 Multiaxial forging (MAF) procedure

MAF at CT was performed on friction screw forging machine at a strain rate of 10 s^{-1}. Successive axial compression of ε=−0.16, which was calculated as an equivalent true strain in one pass ($\Delta\varepsilon$)=ln(1/1.18)= −0.16 and a cumulative strain in one cycle ($\sum\Delta\varepsilon_{n=1}$)=$|\Delta\varepsilon_1+\Delta\varepsilon_2+\Delta\varepsilon_3|$=−0.49 [14] was applied. Extrusion direction of the starting sample was chosen as the first forging axis. Initially, the samples were dipped in liquid nitrogen for 15 min. The samples were then repeatedly forged by changing the axis through 90° in order to maintain the dimensional ratio of 1.18: 1.11: 1.0 at the end of the process. The samples were quenched in liquid nitrogen for 5−10 min after every pass in order to attain thermal equilibrium with liquid nitrogen. The zircaloy-4 samples were subjected to cumulative strains of 1.48, 2.96, 4.44 and 5.91, respectively. The samples were prepared under four different conditions, i.e., 3 cycles (9 passes), 6 cycles (18 passes), 9 cycles (27 passes) and 12 cycles (36 passes). As the alloy failed in shear upon MAF up to 14 cycles, 12 cycles were kept as the highest number of cycles in the present work. Finally, the deformed samples were subjected to annealing at 500 °C for 30 min. To compare the effect at room temperature, the alloy was MAF-treated for the same number of cycles. Samples for investigation of mechanical and microstructural evolution were prepared by sectioning along the plane perpendicular to the last forging axis. The schematic of MAF for 1 cycle and the process are shown in Fig. 1.

2.3 Microstructural characterization

2.3.1 Optical microscopy

Optical microscopy was performed on Leica DMI 5000 microscope under polarized light. Samples were etched with 45% HNO_3 + 45% distilled water + 10% HF for 5−15 s.

2.3.2 Transmission electron microscopy (TEM)

For TEM analysis, FEI-Tecnai 20 G2S – Twin TEM

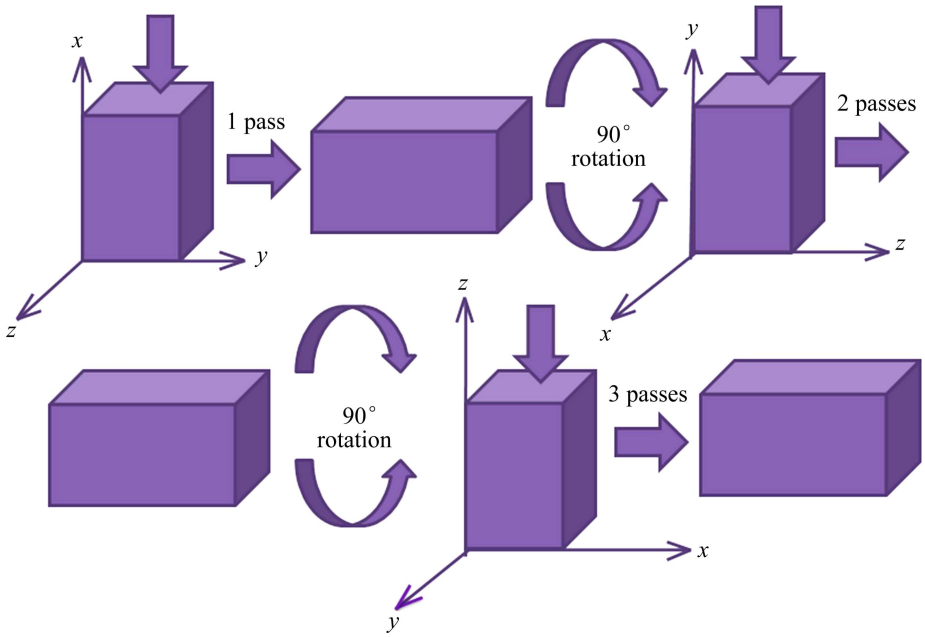

Fig. 1 Schematic of multiaxial forging corresponding to one cycle and MAF process flowchart

operated at 200 kV was used. The samples of zircaloy-4 for TEM study were thinned down to less than 0.1 mm in thickness using 320 to 2000 grit size emery papers and subsequently punched to 3 mm in diameter disk. Thinned foils were twinjet polished at a voltage of 20 V and a temperature of −48 °C in a 20% perchloric acid and 80% methanol solution. The linear intercept method was used to measure the average grain size of the annealed sample.

2.4 X-ray diffraction (XRD)

XRD analysis of MAF-treated zircaloy-4 at CT was performed by advanced X-ray diffraction using Cu K_α radiation with a scan rate of 1 (°)/min. The observed XRD data were analyzed using PANalytical X'Pert HighScore software. The subgrain size (D) and the micro strain $\langle\varepsilon^2\rangle^{1/2}$ were calculated from the integral breadth of the XRD peaks by applying the Williamson−Hall technique [29]. The dislocation density was estimated from the following formula [22,30]:

$$\rho=\frac{2\sqrt{3}}{Db}\langle\varepsilon^2\rangle^{1/2} \quad (1)$$

where b is the Burgers vector and is $1/3[11\bar{2}0]$ [31], and D is the subgrain size.

2.5 Mechanical testing

Tensile tests (H25 K-S Tinius Oslen) of the MAF-treated samples were performed by preparing substandard size specimen with a gauge length of 14 mm at a strain rate of 5×10^{-4} s^{-1} and room temperature. Fractographs of tension test specimens were examined through scanning electron microscopy. Minimum three measurements for each type of MAF-processed zircaloy-4 were taken into consideration during the test. Hardness tests were performed on bulk Vickers hardness tester with a load of 98 N and a dwell time of 15 s at room temperature.

3 Results and discussion

3.1 Microstructure

The optical micrographs of as-received bulk alloy (0 cycle MAF-treated) and MAF-treated alloy up to 6, 9, 12 cycles and 12 cycles followed by annealing at 500 °C for 30 min are shown in Fig. 2. The 0 cycle MAF-treated alloy showed elongated grains with an average grain size of 58 μm (Fig.2 (a)). As the strain was applied, the twin bands were evolved and increased with the cumulative strain/number of cycles. The alloy MAF treated up to 12 cycles, at a cumulative strain of 5.91 in Fig. 2(d) showed a fully deformed microstructure with several twin bands. It is reported that the MAF stimulates the formation of deformation bands in diverse directions, which is contrary to the observation made in this alloy. A high frequency of mutually crossing deformation bands was observed in copper subjected to MDF at 195 K and accumulative strains above 6 [32]. Similar features were observed in MDF of AA6061 alloy at liquid nitrogen temperature (LNT) by RAO et al [14]. The difference in microstructural evolution as a result of MAF of zircaloy-4 at CT might be due to the fact that it is a hexagonal close-packed (HCP) material which has a restricted number of slip systems. After annealing the

MAF-treated zircaloy-4 at 500 °C, it showed a recovered microstructure with several twins crossing the grains (marked with an oval area in Figs. 2(e) and (f)).

Figure 3(a) revealed the presence of α-phase in zircaloy-4, as all the peaks in the pattern match with the reference pattern (98-007−1958) reported for α-phase of zirconium in inorganic crystal structure database (ICSD). The comparative study of XRD peak profiles in

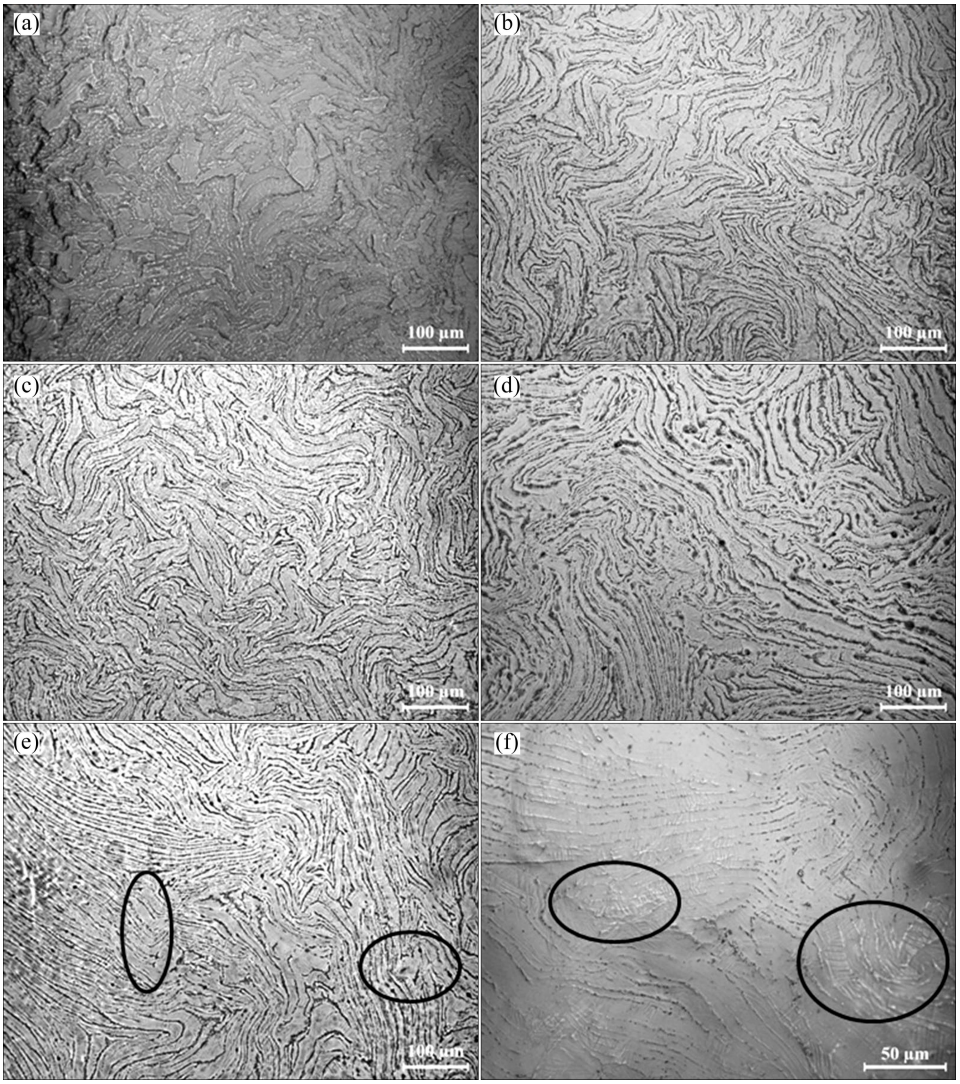

Fig. 2 Optical micrographs of MAF-treated zircaloy-4 subjected to different cumulative strains: (a) 0; (b) 2.96 (6 cycles); (c) 4.44 (9 cycles); (d) 5.91 (12 cycles); (e,f) 12 cycles MAF-treated alloy followed by annealing

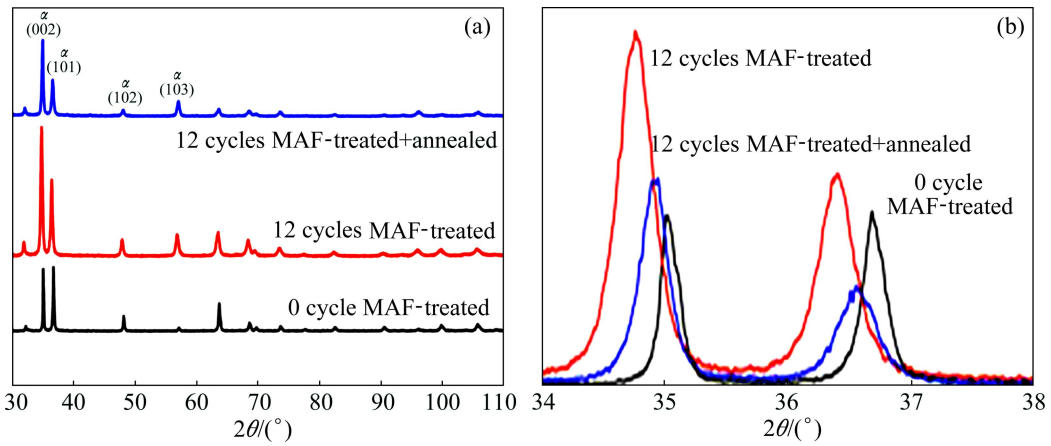

Fig. 3 XRD patterns showing α-phase in MAF-treated zircaloy-4 (0 cycle, 12 cycles and 12 cycles followed by annealing) (a) and showing effect of MAF on peak broadening and shift (b)

Fig. 3(b) revealed peak broadening in the MAF treated samples with the greater broadening in case of 12 cycles deformed sample. It has been reported that peak broadening occurs when the crystal lattice becomes imperfect while cold working. As per the theory of Kinematical scattering, X-ray peak broadening occurs either when particle size is less than a micrometer or if the lattice comprises sufficiently large number of defects, i.e., dislocation density higher than about 5×10^{12} m^{-2} [33]. The dislocation density estimated for as-received alloy is $7.605762\times10^{13}/m^2$. After MAF up to 12 cycles and MAF up to 12 cycles followed by annealing, the dislocation densities observed were $1.762766\times10^{15}/m^2$ and $4.856983\times10^{14}/m^2$, respectively. Further, a small shift in peak towards smaller angles has been noticed, which is attributed to the presence of residual high tensile stresses on application of MAF up to 12 cycles at such a high cumulative strain of 5.91.

3.2 Microstructure evolution mechanism

The TEM micrographs of MAF-treated zircaloy-4 at CT subjected to cumulative strains of 2.96, 4.44 and 5.91 are shown in Fig. 4. Initially, at lower strains, dislocations accumulate in the form of tangles and cell walls. With increasing strain, the dislocations form parallel lamellas with a few dislocation cells, suggesting the effective suppression of dynamic recovery during MAF at CT. The above discussed characteristic features of dislocation boundaries suggest that different deformation mechanisms lead to the evolution of two types of boundaries, viz. incidental boundaries (IDBs), which forms by haphazard entrapment of glide dislocations, and geometrically necessary boundaries (GNBs), which forms between regions favoring different slip activity on the same slip system in order to adjust the co-occurring difference in lattice rotation. The distinction between IDBs and GNBs has been supported by their different capacities to accommodate the amount of misorientations across their boundaries with increasing strain and scaling behavior. At low strains, misorientation angle formed for both types of boundaries is significant. At large strains, dislocations arranged as GNBs can lead to the development of high angle boundaries [34].

In the present work, zircaloy-4 processed by MAF up to 6 cycles at a cumulative strain of 2.96 showed dislocations arranged at cell boundaries, which are also known as IDBs, and low angle grain boundaries (marked by triangles). The less elongated spots in the corresponding SAED pattern in the inset of Fig. 4(a) also substantiated the presence of low angle misorientations among the grains. On increasing the cumulative strain to 4.44 corresponding to 9 cycles, dislocations formed banded structure with dislocation tangles at some location while dislocation cells at other locations

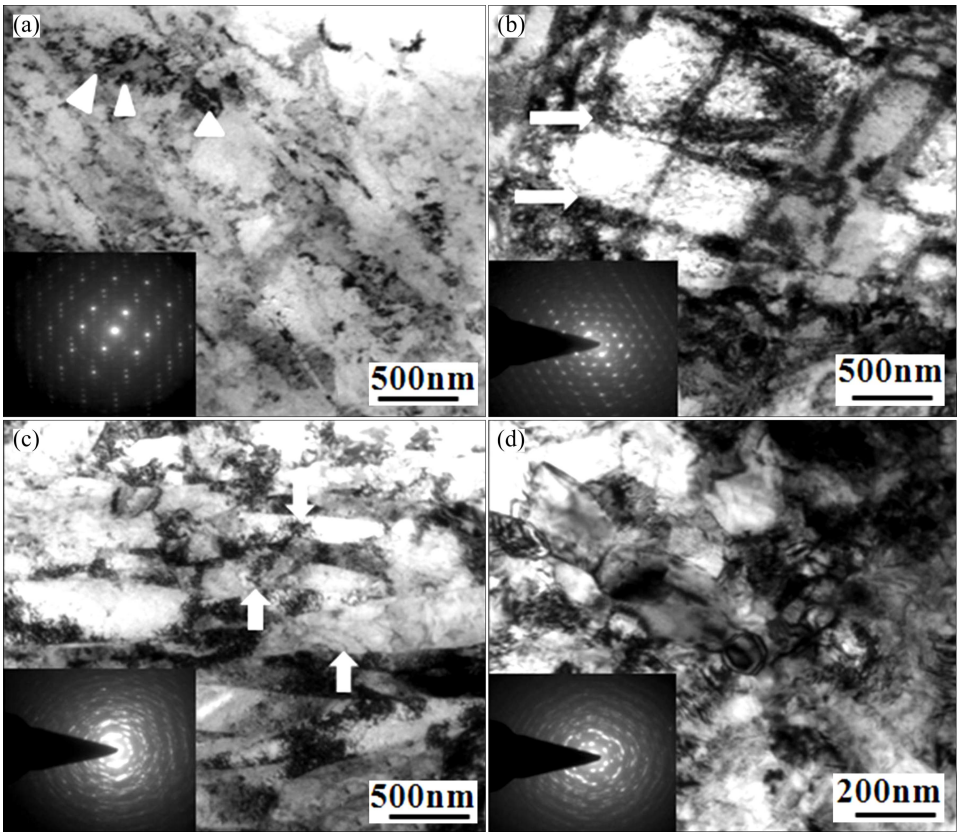

Fig. 4 TEM images of zircaloy-4 after MAF treatment at different cumulative strains: (a) 2.96 (6 cycles); (b) 4.44 (9 cycles); (c) 5.91 (12 cycles); (d) 12 cycles MAF-treated alloy followed by annealing at 500 °C for 30 min

(marked by arrows). At the highest cumulative strain of 5.91 at 12 cycles, the width of the bands decreases to 150−250 nm, thus forming parallel dislocation lamellas (indicated by arrows).

MAF performed at high strain rates stimulated the generation of high density dislocations and restrained their dynamic recovery [21,35], leading to the accumulation and storage of dislocations in the deformed zircaloy-4. In the meantime, the stored high density dislocations interplay with each other at high velocity, thus forming the parallel dislocation lamellas [21,35,36].

The effect of both the forging strain rate and temperature clearly indicates its significance on the microstructure evolution in MAF-treated zircaloy-4, which is defined by a single parameter called Zener–Hollomon parameter (Z) defined as

$$Z = \dot{\epsilon} \exp\left(\frac{Q}{RT}\right) \quad (2)$$

It is reported that the high value of the Z parameter promotes a high stress level [35], which favors the formation and accumulation of dislocations, leading to the evolution of microstructure, resulting in the improvement in mechanical properties of the alloy. It may be mentioned that MAF at CT in the present work was performed at a high Z value (77 K and a strain rate of 10 s^{-1}). Further, annealing zircaloy-4 deformed at 12 cycles at 500 °C for about 30 min, in Fig. 4(d), it undergoes static recovery by rearrangement and annihilation of dislocations, resulting in the formation of stress free equiaxed ultrafine grains. The basis for deciding annealing at 500 °C for 30 min was optimum hardness value and grain refinement with a high degree of misorientation observed at this temperature. The corresponding elongated spots in the discontinuous ring of SAED pattern in the inset showed the high amount of misorientations. This confirms the formation of ultrafine grains of size of 150−250 nm, which is equal to the width of the bands observed at a cumulative strain of 5.91 in the as-deformed alloy. The dynamic recrystallization has not been observed for the deformed zircaloy-4 in the present work. The grains (150−250 nm) with a high density of dislocations were observed after annealing, which is contrary to the results reported in the Refs. [18,32], where dynamic recrystallization had contributed to the grain refinement at cumulative strains above 6.

3.3 Mechanical properties

The variation in hardness and tensile properties of zircaloy-4 processed by MAF at CT is shown in Figs. 5 and 6. With the application of high compressive loads, the dislocation density inside the grains increases, which is proved through an increase in hardness and tensile properties of the deformed samples. Zircaloy-4 MAF processed up to a cumulative strain of 5.91 corresponding to 12 cycles showed an increase in hardness from HV 190 to HV 238 (an increase of 25 %) and ultimate tensile strength increases from 474 to 717 MPa (an increase of 51%). However, the ductility of the deformed alloy has significantly reduced from 18% to

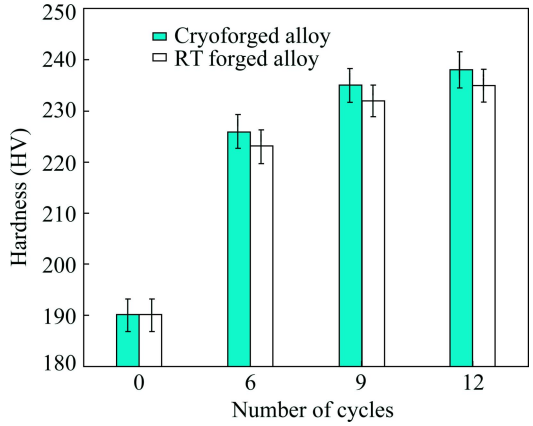

Fig. 5 Variation in hardness of MAF processed zircaloy-4 at CT and room temperature (RT) at 0 cycle, 6 cycles, 9 cycles and 12 cycles

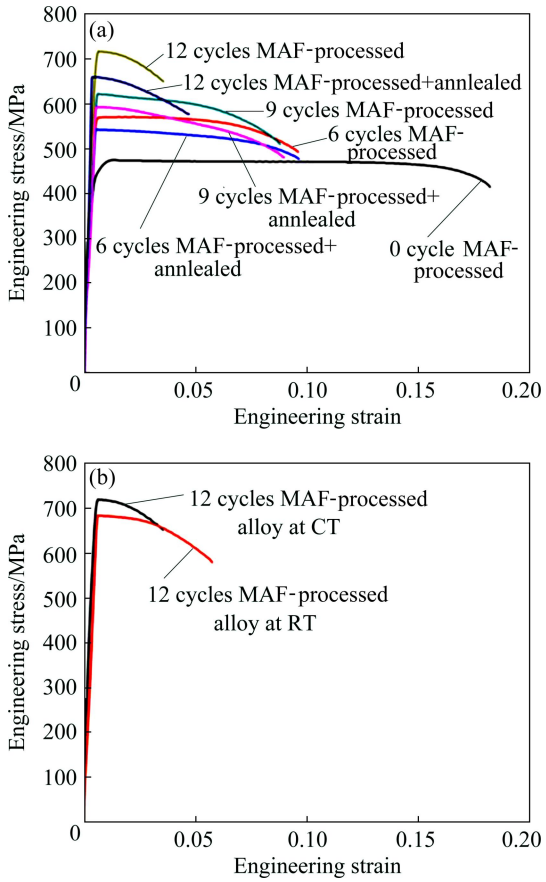

Fig. 6 Variation in stress of MAF-processed and annealed zircaloy-4 at various strain cycles (a) and comparative strength graph of 12 cycles MAF processed alloy at CT and at RT (b)

3.5%, which is attributed to the low strain hardening ability of these severely deformed materials. For comparative analysis, zircaloy-4 was subjected to MAF at the same cumulative strains/number of cycles at room temperature. The 12 cycles MAF-treated alloy at RT showed an increase in hardness from HV 190 to HV 235 (an increase of 24%) (Fig. 5) and an increase in ultimate tensile strength from 474 to 682 MPa (an increase of 44%) (Fig. 6(b)) which was, marginally less as compared with the alloy MAF treated at CT up to the same number of cycles. After annealing the 12 cycles MAF-treated zircaloy-4 at 500 °C for 30 min, it showed a decrease in hardness and tensile strength compared with the same cycle MAF-treated sample, from HV 238 to HV 235 and 717 to 660 MPa, respectively. A marginal increase in ductility from 3.5% to 5% is observed due to recovery which led to the formation of ultrafine grains. Nevertheless, the hardness and the ultimate tensile strength of the annealed alloy were still sufficiently higher (24% and 39%, respectively) than the as-received alloy (0 cycle). It is observed that there is a remarkable increase in strength at the expense of ductility due to grain refinement in metals processed by various severe plastic deformation techniques according to the Hall−Petch relationship [20,37].

The yield strength of the alloy deformed up to 12 cycles has increased from 407 to 666 MPa (63%) and in the case of deformed alloy after annealing; the yield strength has increased from 407 to 627 MPa (54%) which is more as compared with the increase in ultimate tensile strength. On increasing the cumulative strain, the alloy underwent effective strain hardening, which is evident from both the decrease in ductility and less difference between the yield strength and the tensile strength values observed from the tensile tests. The data related to mechanical and microstructural evolution of MAF of zircaloy-4 deformed up to 3 cycles (cumulative strain=1.48) is not shown, as no significant changes in its properties have been noticed. Further, it is reported that the temperature effect on the evolution of strain-induced high angle grain boundaries is insignificant at cumulative strains below 2 [32]. Studies reported on the fabrication of ultrafine grained material via several severe plastic deformation techniques have shown remarkable improvement in tensile strength at the expense of ductility [13,37]. The grain size effect, dislocation density, and solid solution strengthening have contributed to the improvement in tensile strength observed for the MAF-treated zircaloy-4 in the present work.

3.4 Fractographs

The SEM images of fractured surfaces obtained after the tensile test of bulk as-received alloy (0 cycle MAF-treated) and the MAF-treated alloy (12 cycles and 12 cycles followed by annealing) are shown in Fig. 7. The micrograph of as-received bulk alloy showed large sized dimples attributed to the high ductility (~18% elongation). On MAF up to 12 cycles, the alloy showed dimples all over the surface with reduced size equal to submicron level. The SEM micrograph of MAF treated and annealed alloy also depicted a large number of dimples with a size slightly larger than that shown by deformed alloy which is due to the annealing effect. It is reported that the void initiation site and the number of voids initiated at the grain boundaries are related to the

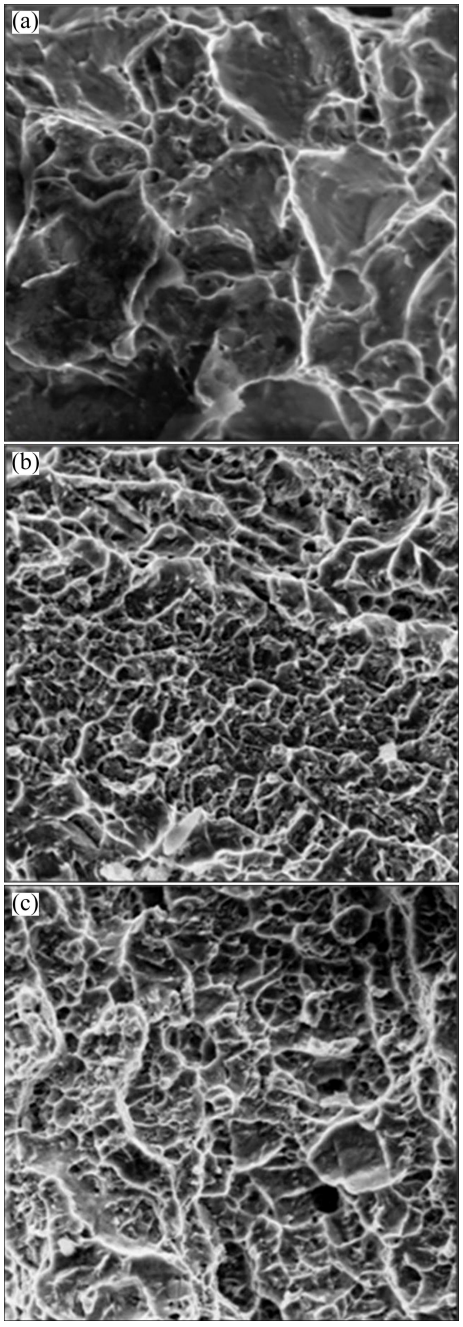

Fig. 7 Micrographs of MAF-treated zircaloy-4 at different cumulative strains: (a) 0; (b) 5.91 (12 cycles); (c) 12 cycles MAF-treated alloy followed by annealing

dimple size [14,38]. Therefore, grain refinement during MAF at CT has led to the development of small sized dimples.

4 Conclusions

1) MAF up to 12 cycles showed improvement in hardness from HV 190 to HV 238 (25%), while increment in tensile strength from 474 to 717 MPa (51%) and yield strength from 407 to 666 MPa (63%) was observed.

2) The hardness decreases from HV 238 to HV 235 and tensile strength from 717 to 660 MPa after annealing the alloy deformed at the highest cumulative strain (5.91) at 500 °C for 30 min, which are still higher (24% and 39%) than the as-received alloy.

3) The dislocation density increases with the increase in cumulative strain, with the highest dislocation density estimated in the alloy deformed at the highest cumulative strain (5.91). The alloy after annealing reveals recovery process leading to the formation of ultrafine grains with sizes of 150−250 nm.

4) Fractured surfaces of the 12 cycles MAF treated alloy and the alloy MAF treated followed by annealing exhibit dimple features which are a characteristic of ductile fracture and the reduction in dimple size substantiated the grain refinement.

Acknowledgements

One of the authors, Dr. R. JAYAGANTHAN, would like to thank BRNS, Bombay for their financial grant to this work through grant No. BRN-577-MMD.

References

[1] VALIEV R Z, ESTRIN Y, HORITA Z, LANGDON T G, ZECHETBAUER M J, ZHU Y T. Producing bulk ultrafine-grained materials by severe plastic deformation [J]. Journal of the Minerals Metals and Materials Society, 2006, 58: 33−39.

[2] ZRNIK J, DOBATKIN S V, MAMUZIČ I. Processing of metals by severe plastic deformation (SPD) — Structure and mechanical properties respond [J]. Metalurgija, 2008, 47: 211−216.

[3] SOLIMAN M S, EL-DANAF E A, ALMAJID A A. Effect of equal-channel angular pressing process on properties of 1050 Al alloy [J]. Materials and Manufacturing Processes, 2012, 27: 746−750.

[4] RAEI M, TOROGHINEJAD M R, JAMAATI R. Nano/ultrafine structured AA1100 by ARB process [J]. Materials and Manufacturing Processes, 2011, 26: 1352−1356.

[5] YU H L, LU C, TIEU A K, KONG C. Fabrication of nanostructured aluminum sheets using four-layer accumulative roll bonding [J]. Materials and Manufacturing Processes, 2014, 29: 448−453.

[6] THAM Y W, FU M W, HNG H H, PEI Q X, LIM K B. Microstructure and properties of Al-6061 alloy by equal channel angular extrusion for 16 passes [J]. Materials and Manufacturing Processes, 2007, 22: 819−824.

[7] FU M W, YONG M S, PEI Q X, HNG H H. Deformation behavior study of multi-pass ecae process for fabrication of ultrafine or nanostructured bulk materials [J]. Materials and Manufacturing Processes, 2006, 21: 507−512.

[8] DAS D, SAMANTA A, CHATTOPADHYAY P P. Deformation behavior of bulk ultrafine grained copper prepared by sub-zero rolling and controlled recrystallization [J]. Materials and Manufacturing Processes, 2006, 21: 698−702.

[9] ESTRIN Y, VINOGRADOV A. Extreme grain refinement by severe plastic deformation: A wealth of challenging science [J]. Acta Materialia, 2013, 61: 782−817.

[10] HAN B J. Ultrafine grained Fe−32% Ni alloy processed by multiaxial forging [J]. Advanced Materials Research, 2010, 97: 187−190.

[11] MIURA H, MARUOKA T, YANG X, JONAS J J. Microstructure and mechanical properties of multi directionally forged Mg−Al−Zn alloy [J]. Scripta Materialia, 2012, 66: 49−51.

[12] MIURA H, MARUOKA T, JONAS J J. Effect of ageing on microstructure and mechanical properties of a multi-directionally forged Mg−6Al−1Zn alloy [J]. Materials Science and Engineering A, 2013, 563: 53−59.

[13] PADAP A K, CHAUDHARI G P, PANCHOLI V, NATH S K. Warm multiaxial forging of AISI 1016 steel [J]. Materials and Design, 2010, 31: 3816−3824.

[14] RAO P N, SINGH D, JAYAGANTHAN R. Mechanical properties and microstructural evolution of Al 6061 alloy processed by multidirectional forging at liquid nitrogen temperature [J]. Materials and Design, 2014, 56: 97−104.

[15] CHERUKURI B, SRINIVASAN R. Properties of AA 6061 processed by multi axial compression/forging (MAC/F) [J]. Materials and Manufacturing Processes, 2006, 21: 519−525.

[16] TANG L, LIU C, CHEN Z, JI D, XIAO H. Microstructures and tensile properties of Mg−Gd−Y−Zr alloy during multidirectional forging at 773 K [J]. Materials and Design, 2013, 50: 587−596.

[17] ZHEREBTSOV S, KUDRYAVTSEV E, KOSTJUCHENKO S, MALYSHEVA S, SALISHCHEV G. Strength and ductility-related properties of ultrafine grained two-phase titanium alloy produced by warm multiaxial forging [J]. Materials Science and Engineering A, 2012, 536: 190−196.

[18] BELYAKOV A, SAKAI T, MIURA H, TSUZAKI K. Grain refinement in copper under large strain deformation [J]. Philosophical Magazine A, 2001, 81: 2629−2643.

[19] WU X, GONG Y, REN S, TAO J, LONG Y, CHENG L, ZHU X. Effect of annealing on mechanical properties of copper alloys deformed at cryogenic temperature [J]. Materials Science Forum, 2013, 745−746: 363−370.

[20] HANSEN N. Hall−Petch relation and boundary strengthening [J]. Scripta Materialia, 2004, 51: 801−806.

[21] GUO D, LI M, SHI Y, ZHANG Z, ZHANG H, LIU X, ZHANG X. Effect of strain rate on microstructure evolutions and mechanical properties of cryorolled Zr upon annealing [J]. Materials Letters, 2012, 66: 305−307.

[22] GUO D, LI M, SHI Y, ZHANG Z, ZHANG H, LIU X, WEI B, ZHANG X. High strength and ductility in multimodal structured zirconium [J]. Materials and Design, 2012, 34: 275−278.

[23] GUO D, ZHANG Z, ZHANG G, LI M, SHI Y, MA T, ZHANG X. An extraordinary enhancement of strain hardening in fine-grained zirconium [J]. Materials Science and Engineering A, 2014, 591: 167−172.

[24] SHI Y, LI M, GUO D, MA T, ZHANG Z, ZHANG G, ZHANG X. Tailoring grain size distribution for optimizing strength and ductility of multimodal zirconium [J]. Materials Letters, 2013, 108: 228−230.

[25] KAMALNATH P A R, SARKAR A. Tensile behavior of cryorolled zircaloy-2 [J]. American Journal of Materials Science, 2012, 2: 138−141.

[26] MURTY K L, CHARIT I. Texture development and anisotropic deformation of zircaloys [J]. Progress in Nuclear Energy, 2006, 48: 325−359.
[27] GANGULY C. Advances in zirconium technology for nuclear reactor applications [C]//DE P K. Proc of the Symposium Zirconium 2002. Mumbai, India: INIS, 2002: 1−27.
[28] MANI KRISHNA K V, SAHOO S K, SAMAJDAR I, NEOGY S, TEWARI R, SRIVASTAVA D, DEY G K, HARI D G, SAIBABA N, BANARJEE S. Microstructural and textural developments during zircaloy-4 fuel tube fabrication [J]. Journal of Nuclear Materials, 2008, 383: 78−85.
[29] SARKAR A, MUKHERJEE P, BARAT P. X-ray diffraction studies on asymmetrically broadened peaks of heavily deformed zirconium-based alloys [J]. Material Science and Engineering A, 2008, 485: 176−181.
[30] WILLIAMSON G K, SMALLMAN R E. Dislocation densities in some annealed and cold worked metals from measurements on the X-ray Debye−Scherrer spectrum [J]. Philosophical Magazine, 1956, 1: 34−46.
[31] LEE C S, KO Y G, SHIN D H. An analysis of the strain hardening behavior of ultrafine grain pure titanium [J]. Scripta Materialia, 2006, 54: 1785−1789.
[32] DIETER G E. Mechanical metallurgy [M]. METRIC S I. London: McGraw-Hill, 1988.
[33] KOBAYASHI C, SAKAI T, BELYAKOV A, MIURA H. Ultrafine grain development in copper during multidirectional forging at 195 K [J]. Philosophical Magazine Letters, 2007, 87: 751−766.
[34] UNGÁR T. Microstructural parameters from X-ray diffraction peak broadening [J]. Scripta Materialia, 2004, 51: 777−781.
[35] HUGHES D A, HANSEN N, BAMMANN D J. Geometrically necessary boundaries, incidental dislocation boundaries and geometrically necessary dislocations [J]. Scripta Materialia, 2003, 48: 147−153.
[36] HUANG F, TAO N R, LU K. Effects of strain rate and deformation temperature on microstructures and hardness in plastically deformed pure aluminum [J]. Journal of Materials Science and Technology, 2011, 27: 1−7.
[37] WANG K, TAO N R, LIU G, LU J, LU K. Plastic strain-induced grain refinement at the nanometer scale in copper [J]. Acta Materialia, 2006, 54: 5281−5291.
[38] GOEL S, JAYAGANTHAN R, SINGH I V, SRIVASTAVA D, DEY G K, SAIBABA N. Mechanical and microstructural characterizations of ultrafine grained zircaloy-2 produced by room temperature rolling [J]. Materials and Design, 2014, 55: 612−618.

低温多向锻造锆-4 合金的力学性能和超细晶组织演化

D. FULORIA[1], S. GOEL[1], R. JAYAGANTHAN[1], D. SRIVASTAVA[2], G. K. DEY[2], N. SAIBABA[3]

1. Department of Metallurgical and Materials Engineering, Centre of Nanotechnology IIT Roorkee, Roorkee 247667, India;
2. Materials Science Division, Bhabha Atomic Research Center, Mumbai 40085, India;
3. Nuclear Fuel Complex Limited, Hyderabad 501301, India

摘　要：研究低温(77 K)多向锻造锆-4 合金累积应变为 1.48，2.96，4.44 和 5.91 时的力学性能和组织演变。通过万能拉伸测试和维氏硬度实验测得多向锻造合金的力学性能。相对于原始合金，当锆-4 合金变形的累积变形为 5.91 时，其极限抗拉强度从 474 MPa 提高到 717 MPa， 维氏硬度从 HV 190 提高到 HV 238。然而，由于锆-4 合金的低应变硬化，其延展性显著降低(18%~3.5%)。变形合金强度和硬度的提高是因为多向锻造引起的晶粒尺寸效应和高的位错密度。采用光学显微镜和透射电镜表征变形试样的显微组织演化。当累积应变为 5.91 时，经 12 次多向锻造后合金的微观组织演化主要是超细晶的形成，其平均晶粒尺寸为 150~250 nm。

关键词：锆-4 合金；多向锻造；低温；超细晶；显微组织演变；力学性能

(Edited by Xiang-qun LI)